Xenon and Halogenated Alkanes Track Putative Substrate Binding Cavities in the Soluble Methane Monooxygenase Hydroxylase[†,‡]

Douglas A. Whittington,[§] Amy C. Rosenzweig,[§,⊥] Christin A. Frederick,[*,⊥] and Stephen J. Lippard[*,§]

Department of Chemistry, Massachusetts Institute of Technology, Cambridge, Massachusetts 02139 and Department of Biological Chemistry and Molecular Pharmacology, Harvard Medical School and Dana Farber Cancer Institute, Boston, Massachusetts 02115

Received September 25, 2000; Revised Manuscript Received January 10, 2001

ABSTRACT: To investigate the role of protein cavities in facilitating movement of the substrates, methane and dioxygen, in the soluble methane monooxygenase hydroxylase (MMOH), we determined the X-ray structures of MMOH from *Methylococcus capsulatus* (Bath) cocrystallized with dibromomethane or iodoethane, or by using crystals pressurized with xenon gas. The halogenated alkanes bind in two cavities within the α-subunit that extend from one surface of the protein to the buried dinuclear iron active site. Two additional binding sites were located in the *β*-subunit. Pressurization of two crystal forms of MMOH with xenon resulted in the identification of six binding sites located exclusively in the α-subunit. These results indicate that hydrophobic species bind preferentially in preexisting cavities in MMOH and support the hypothesis that such cavities may play a functional role in sequestering and enhancing the availability of the physiological substrates for reaction at the active site.

The biological oxidation of methane occurs at a carboxylate-bridged dinuclear iron active site located in the 251-kDa hydroxylase component (MMOH) of the soluble methane monooxygenase enzyme system (sMMO)[1] (*1*, *2*). The question has arisen why nature would choose such a large enzyme to process such small substrates as CH_4 and O_2. The structure of MMOH from two organisms, *Methylococcus capsulatus* (Bath) and *Methylosinus trichosporium* OB3b, is known (*3*, *4*). MMOH exists as an $\alpha_2\beta_2\gamma_2$ homodimer with each α-subunit housing one diiron unit (*3*). Dioxygen and methane interact with the dinuclear iron center in a strategically positioned hydrophobic cavity at the active site. These nonpolar substrates are converted to the much more hydrophilic product molecules, methanol and water. The different dielectric constants of the substrate and product molecules for MMOH suggest one reason such a large protein may be required for catalysis, namely, the need to control the traffic of species with such diverse polarity through noninterfering pathways in the enzyme. The large size of MMOH may also be needed to bind two other component proteins of the sMMO system. Electrons required for the mixed function oxidation are supplied by NADH via the reductase (MMOR) component. The dinuclear iron center in MMOH is converted from Fe(III)Fe(III) to Fe(II)Fe(II) by transfer of electrons from MMOR (*5*). A third component, protein B (MMOB), couples the system to perform monooxygenase chemistry when substrates are present (*6*, *7*).

The dinuclear iron active site resides in a four-helix bundle within the α-subunit, buried beneath the protein surface. A number of hydrophobic cavities have been identified by analysis of the MMOH structure, with several in the α-subunit forming a putative pathway from the protein surface to the active site (Figure 1) (*3*, *8*). The amino acids lining cavities 2 and 3 are primarily hydrophobic, suggesting that they may be functionally important for guiding dioxygen and methane to cavity 1 at the catalytic diiron center. Other metalloproteins that process gases for transport or redox functions, such as myoglobin and a Ni-Fe hydrogenase, similarly contain hydrophobic cavities that can accommodate the gaseous substrates (*9*, *10*).

In the present work, we applied X-ray crystallography in conjunction with the use of heavy atom substrate probes to address the hypothesis that the hydrophobic cavities in MMOH might be functionally important. Since methane itself is difficult to identify in protein electron density maps, being indistinguishable from water, we used dibromomethane and iodoethane as surrogates in cocrystallization experiments and xenon in crystal pressurization experiments. The choice of xenon was particularly appropriate for investigating methane binding since the two have very similar van der Waals radii (∼2.15 Å). The resulting structures revealed discrete binding sites for all of these species in MMOH. In every structure, cavities 2 and 3 housed exogenous molecules. Additional

[†] Funding was provided by National Institutes of Health Research Grants GM32134 (S.J.L.) and GM48388 (S.J.L. and C.A.F.). This work is based upon research conducted at the Stanford Synchrotron Radiation Laboratory (SSRL), which is funded by the Department of Energy (BES, BER) and the National Institutes of Health (NCRR, NIGMS). D.A.W. was supported in part by an NIH Biotechnology Predoctoral Traineeship.

[‡] Coordinates have been submitted to the RCSB for the MMOH structures containing dibromomethane (1FZ8), iodoethane (1FZ9), and xenon (1FZI and 1FZH for crystal forms 1 and 2, respectively).

* To whom correspondence should be addressed. S.J.L., Tel: 617-253-1892, FAX: 617-258-8150, E-mail: lippard@lippard.mit.edu. C.A.F., Tel: 617-632-3984, FAX: 617-632-4393, E-mail: caf@red.dfci.harvard.edu.

[§] Massachusetts Institute of Technology.

[⊥] Harvard Medical School and Dana Farber Cancer Institute.

[1] Abbreviations: sMMO, soluble methane monooxygenase; MMOH, methane monooxygenase hydroxylase; MMOB, methane monooxygenase protein B; MMOR, methane monooxygenase reductase; NADH, reduced nicotinamide adenine dinucleotide.

10.1021/bi0022487 CCC: $20.00
Published on Web 03/01/2001

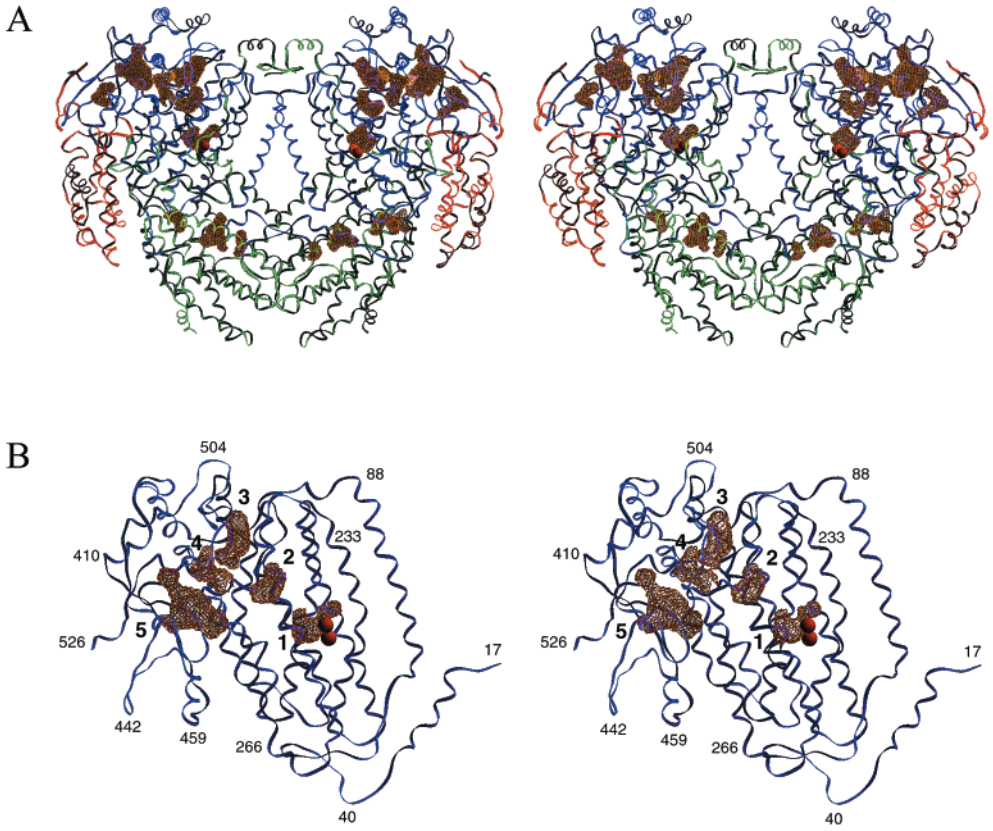

FIGURE 1: (A) Stereoview of the MMOH structure showing the location of cavities with a volume ≥ 40 Å^3, as determined by VOIDOO (*18*). The brown net surfaces depict the cavities, and the α-, *β*-, and *γ*-subunits are blue, green, and red, respectively. The iron atoms are depicted as red spheres. (B) Stereoview of the α-subunit depicting the cavities considered to be important for substrate binding and access to the active site. The iron atoms are shown as red spheres, and the cavities are numbered 1 through 5. Smaller numbers indicate the locations of various amino acids in the α-subunit sequence.

binding sites for xenon were present in the α-subunit, and dibromomethane and iodoethane molecules also occupied locations in the *β*-subunits.

EXPERIMENTAL PROCEDURES

Protein Purification and Crystallization. Hydroxylase was purified from native *M. capsulatus* (Bath) cells as described previously (*11*). MMOH crystals in form II were grown by hanging drop vapor diffusion at room temperature as described (*12*). Microseeding was used to obtain improved crystals for data collection. Solutions for cocrystallizing MMOH with CH_2Br_2 or CH_3CH_2I were 25%-saturated with these species. Form I crystals of MMOH were grown as reported (*13*).

Data Collection and Refinement. High-resolution data were collected at 100 K on beamline 7-1 of the Stanford Synchrotron Radiation Laboratory (SSRL) using $\lambda = 1.08$ Å and a Mar Research imaging plate detector. Data were indexed and scaled with the HKL suite of programs (*14*). Data collection statistics appear in Table 1.

Structure determinations were initiated by using the native coordinates and phases from MMOH in the appropriate crystal form as a starting model in rigid body refinement in CNS (v. 1.0) (*15*). Cycles of positional, simulated-annealing, and B-factor refinements were run, interspersed with analysis of the geometry of the model and with manual rebuilding into electron density. Manual rebuilding was performed in O (*16*). The locations of exogenous CH_2Br_2, CH_3CH_2I, and Xe in the structure were identified by the presence of large features of electron density in maps generated with the Fourier coefficients $||F_{obs,\ ligand}| - |F_{obs,\ native}||$ using phases from the native structure. Solvent was added by four or five rounds of automated water picking followed by manual inspection of the selected peaks. Occupancies of the haloalkane species and of the xenon atoms were calculated by setting the B-values for these species equal to the overall B-values of the solvent molecules in the structure. A single round of positional refinement was then run, followed by refinement of individual B-values for all atoms in the model. Occupancy refinements were not run on the 3.3 Å data for crystal form I MMOH. Geometries of the model during the course of the refinements were assessed with PROCHECK (*17*). Refinement statistics are listed in Table 1.

Cavity Characterization. Molecular volumes, cavity locations, and cavity volumes were determined initially by using the program VOIDOO (*18*). A 1.2 Å sphere was used to generate the probe accessible surface on a 0.40 Å grid. Multiple, random orientations of individual MMOH subunits were used as input for the VOIDOO program to generate multiple measures of the volumes, as suggested by the program's authors (*18*). Cavity volumes were also calculated by using the server-based program CAST (*19*).

Xe Pressurization of Crystals. Pressurization with xenon gas was carried out at beamline 7-1 of SSRL using apparatus that has been described previously (*20*). Crystals of MMOH in both crystal form I and crystal form II were harvested into stabilizing solutions and transported to SSRL. Small magnetic mounts containing fiber loops were used to pick a

Table 1: X-ray Data Collection and Refinement Statistics

	$MMOH_{chbr}$	$MMOH_{eti}$	$MMOH_{xe2}$	$MMOH_{xe1}$
space group	$P2_12_12_1$	$P2_12_12_1$	$P2_12_12_1$	$P2_12_12_1$
cell constants *a*, *b*, *c* (Å)	71.2, 172.0, 221.3	71.2, 172.2, 221.2	72.3, 174.6, 223.0	61.7, 109.6, 330.2
resolution range (Å)	30−2.10	30−2.30	30−2.60	12−3.30
total no. of reflections measured	654 647	919 602	552 751	340 070
no. of unique reflections	136 846	107 645	81 746	25 369
R_{sym} (%)[a] (highest shell)	8.4 (55.5)	7.8 (40.4)	10.5 (28.1)	11.1 (21.9)
completeness (%) (highest shell)	86.0 (85.3)	86.8 (83.9)	93.2 (96.6)	74.0 (69.9)
resolution range used for refinement (Å)	30−2.10	30−2.30	30−2.60	12−3.30
no. of reflections used for refinement	123 585	91 903	75 732	23 398
R-factor (%)[b]	20.1	20.5	20.6	22.3
R_{free} (%)[c]	25.0	25.9	26.0	25.3
rms deviations				
bond lengths (Å)	0.006	0.006	0.007	0.01
bond angles (°)	1.17	1.21	1.23	1.51

[a] $R_{sym} = \Sigma |I - \langle I \rangle| / \Sigma I$, where I is the observed intensity and $\langle I \rangle$ is the average intensity over all observations of symmetry-related reflections. [b] R-factor $= \Sigma |F_{obs} - F_{calc}| / \Sigma F_{obs}$, where F_{obs} and F_{calc} are the observed and calculated structure factor amplitudes, respectively. [c] R_{free} was calculated from a randomly chosen subset of 4.5% of the reflections.

crystal out of the cryosolution. The magnetic mount containing the crystal was lowered into the pressurization chamber that contained ~500 μL of mother liquor at the base of the cell. The chamber was capped and the atmosphere was purged three times with 50 psi xenon gas. For crystals of form II, the chamber was then pressurized to 100 psi (6.8 atm) and equilibrated for 15 min. After the equilibration period, the cell was vented by rapidly unscrewing the cap, and a magnetic wand was used to pick up the crystal on the magnetic mount and plunge it into liquid nitrogen. Using two people, the entire process from venting to freezing took 4−5 s. For crystals of form I, this same pressurization and plunge-freezing procedure resulted in damaged crystals. Consequently, after purging the chamber, form I crystals were pressurized at 60 psi (4.1 atm) for only 5 min. The chamber was vented as before and the crystal was flash-frozen directly in the cold nitrogen stream. This procedure took ~8 s from venting to freezing.

RESULTS

Cocrystallization of MMOH with Halogenated Alkanes. Crystal structures of MMOH containing CH_2Br_2 and CH_3CH_2I were solved to 2.1 and 2.3 Å resolution, respectively, and several distinct binding sites were identified (Figure 2). Both species occupy cavities 2 and 3 in each α-subunit (Figure 3), as well as two sites in each β-subunit. The only significant difference between the two structures is that cavity 2 houses two dibromomethane molecules but only one iodoethane molecule. Both CH_2Br_2 and CH_3CH_2I have molecular volumes of ~62 Å^3, so this difference may be a consequence of their respective dipole moments. Dibromomethane has the larger dipole moment and binds in van der Waals contact with Phe290 (Figure 3), analogous to the binding of haloalkanes in enzymes such as haloalkane dehalogenase (*21*). Peak heights and the corresponding refined occupancy and B-values for the dibromomethane and iodoethane species are given in Tables 2 and 3, respectively.

α-Subunit Binding Sites for CH_2Br_2 and CH_3CH_2I. Binding within the α-subunit cavities caused very little structural rearrangement of the native protein. In cavity 2, van der Waals contacts between CH_2Br_2 or CH_3CH_2I and surrounding amino acids nudged Leu110 toward the active site cavity, causing it to adopt the rotameric conformation found in crystal form I (*8*). Slight rearrangements also occurred in the orientations of Phe188, which separates cavities 1 and 2, and Leu289 and Phe290, which line cavity 2. The conformations of the other amino acids lining cavity 2 were unaltered.

Table 2: CH_2Br_2 Binding Sites in MMOH

site	peak heights for Br atoms (σ)[a]	location[b]	occupancy	B-values
1	41.2	α2, cavity 3	1.00	28.9
	38.5		1.00	27.5
2	37.8	α1, cavity 3	1.00	29.4
	36.5		1.00	30.4
3	32.9	β1, inner	0.89	32.1
	31.2		0.89	29.7
4	30.4	α2, cavity 2	0.79	29.5
	30.2		0.79	34.3
5	30.0	β2, inner	0.79	34.7
	29.2		0.79	28.5
6	29.3	α1, cavity 2	0.79	30.4
	26.1		0.79	35.2
7	24.1	α2, cavity 2	0.64	27.3
	22.7		0.64	33.0
8	22.6	α1, cavity 2	0.58	28.2
	20.2		0.58	29.3
9	11.4	β1, outer	0.44	34.2
	10.3		0.44	38.8
10	9.3	β2, outer	0.34	40.0
	6.2		0.34	42.4

[a] Peak heights are in reference to a difference map calculated with the coefficients $||F_{o,\,dibromomethane}| - |F_{o,\,native}||$ with phases from the native structure (ref *12*). [b] α1 and α2 refer to the alpha subunit of protomers 1 and 2, respectively.

Table 3: CH_3CH_2I Binding Sites in MMOH

site	peak heights for *I* atoms (σ)[a]	location[b]	occupancy	B-values
1	50.6	α2, cavity 3	0.97	39.9
2	46.8	α1, cavity 3	0.87	38.3
3	36.0	β1, inner	0.73	39.8
4	33.9	β2, inner	0.60	40.4
5	23.3	α1, cavity 2	0.52	40.6
6	22.9	α2, cavity 2	0.50	41.4
7	15.5	β1, outer	0.35	38.5
8	11.6	β2, outer	0.27	42.2

[a] Peak heights are in reference to a difference map calculated with the coefficients $||F_{o,\,iodoethane}| - |F_{o,\,native}||$ with phases from the native structure (ref *12*). [b] α1 and α2 refer to the alpha subunit of protomers 1 and 2, respectively.

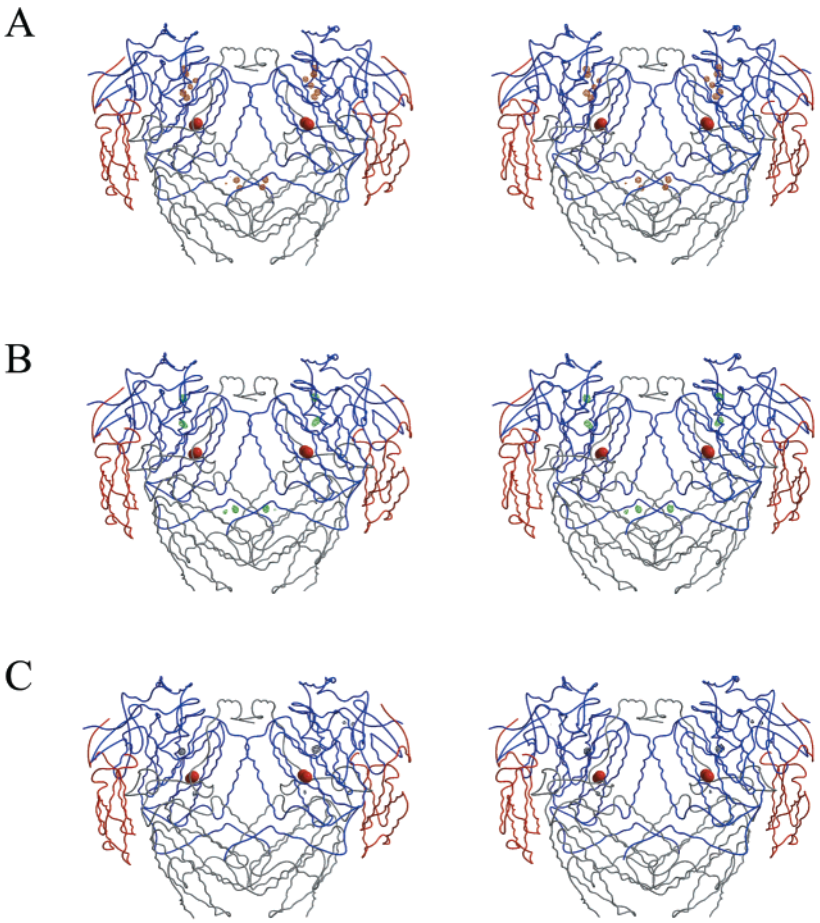

FIGURE 2: Stereoviews of the MMOH structure showing peaks of significant difference electron density in maps calculated with the Fourier coefficients $||F_{o,\ ligand}| - |F_{o,\ native}||$ from the native structure. The α-, β-, and γ-subunits are depicted in blue, gray, and red, respectively, and peaks are shown for the (A) dibromomethane structure (orange, contoured at 10σ), (B) iodoethane structure (green, contoured at 10σ), and (C) 2.6 Å resolution xenon structure (black, contoured at 5σ).

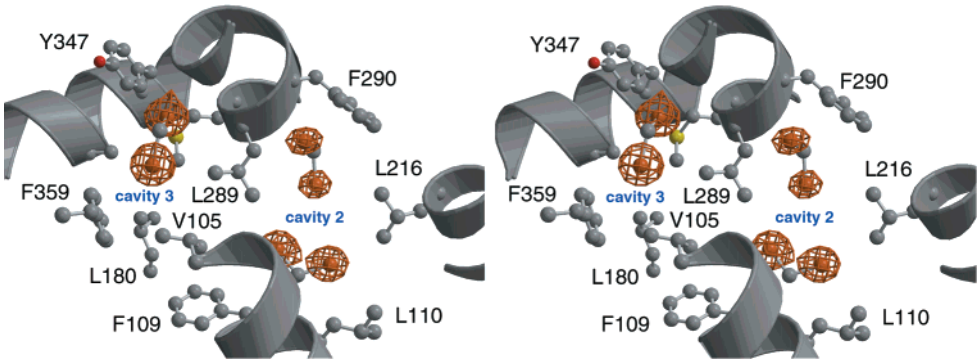

FIGURE 3: Stereoview of the dibromomethane binding sites in cavities 2 and 3 of the α-subunit. Difference electron density peaks (orange, 10σ contour) are shown for maps calculated with the Fourier coefficients $||F_o| - |F_c||$ using phases from the final model minus the dibromomethane molecules. Superimposed on these peaks are the dibromomethane molecules from the final model. Individual bromine atoms are clearly delineated in the maps.

Binding of CH_2Br_2 or CH_3CH_2I in cavity 3 similarly caused little perturbation of surrounding amino acid side chains. The only conformational variation was that of Leu289, which together with Met288 and Val105 separates cavities 2 and 3. Despite its largely hydrophobic nature, two water molecules reside in cavity 3 in the native structure, forming hydrogen bonds to the backbone carbonyl groups of Tyr292 and Arg360, the backbone amide of Ala362, and to each other. The remainder of the cavity is empty. Upon binding of either CH_2Br_2 or CH_3CH_2I, the void is filled but the two water molecules remain with the identical hydrogen bonding interactions. The positions of CH_2Br_2 and CH_3CH_2I within each cavity are very similar, resulting in nearly identical van der Waals contacts with the surrounding protein.

Examination of the remaining cavities in the α-subunit (Figure 1, panel B) revealed no electron density attributable to a halogenated alkane. Ordered water molecules bind in cavity 5, as in the native structure. Since cavities 4 and 5 have a more hydrophilic composition, the observed results indicate a preference of small halogenated alkanes for binding in the more hydrophobic environments. Such behavior has been encountered previously in other proteins. Dichloro-

methane binds in hydrophobic cavities in myoglobin and hemoglobin, and dichloroethane binds to insulin (*22*−*24*).

β-Subunit Binding Sites for CH_2Br_2 and CH_3CH_2I. The CH_2Br_2 and CH_3CH_2I derivatized proteins reveal the presence of two haloalkane binding sites in each β subunit of MMOH, located at the β−β interface and related to one another by a noncrystallographic 2-fold rotation axis. A shallow pocket on the protein surface defines these closely related binding sites. The innermost site is lined by amino acids Glu116, Thr286, and Gln283 from one β-subunit, and Tyr119, Arg122, and Phe123 from the other β-subunit. Upon CH_2Br_2 or CH_3CH_2I binding, the only significant structural rearrangement is rotation of the Tyr119 phenyl rings from adjacent β-subunits by ∼90°. In this altered orientation, the two rings are parallel and located ∼3.8 Å apart, suggesting possible π−π stacking. The outer binding site in each β-subunit was more weakly occupied. At this position, the haloalkanes make van der Waals contacts to the side chains of Gln125 and Arg122 and the backbone of Gln125 and Gly126 from one β-subunit, as well as to Ile290, Thr286, and Gln293 from the other β-subunit.

Xe Pressurization of MMOH Crystals. Crystals of MMOH grown in the two different forms reported previously were exposed to moderate pressures (6.8 atm) of xenon gas as a probe for methane binding in the protein. Like methane, xenon is a nonpolar, water-soluble gas. The two have very similar van der Waals radii, but xenon contains many more electrons making it much easier to identify in electron density maps. Prior reports indicate that xenon binds in hydrophobic cavities in proteins (*9*, *10*, *25*, *26*). Pressurization for 15 min followed by rapid depressurization and flash-freezing of the crystals allowed us to determine structures to 3.3 and 2.6 Å resolution for the first and second crystal forms of MMOH, respectively. The diffraction resolution of both form I and II crystals decreased, and the mosaicities increased, during the pressurization treatment. This behavior reflects dehydration of crystals suspended in loops for >15 min, although steps were taken to prevent excessive solvent loss (see Experimental Procedures).

A total of nine peaks were identified in initial difference maps calculated with the Fourier coefficients $||F_{obs,\ ligand}| - |F_{obs,\ native}||$ using phases from the native structure (Figure 2, panel C). Subsequent refinements led to the identification of 11 distinct xenon binding sites in the α-subunits of MMOH (Table 4). Two α-subunit binding sites corresponded to cavity 2 where CH_2Br_2 and CH_3CH_2I also bind (Figure 4, panel A). Cavity 3 in one protomer also contained a xenon atom in the position where the haloalkanes were located. The other protomer displayed a feature of electron density in cavity 3 indicative of three distinct but overlapping sites. In contrast to the haloalkane structures, xenon binding did not alter the conformation of Leu110 or other residues lining cavities 2 and 3.

Three additional α-subunit Xe-binding sites were also identified. Two appeared 4.2 Å from each other in a hydrophobic pocket on the protein surface defined by residues Phe519, Cys517, Leu478, Leu405, Leu353, and Pro355 (Figure 4, panel B). The only rearrangement observed was an alternate rotamer for Cys517. These locations lie adjacent to cavity 4 and, together with the sites in cavities 2 and 3, trace a putative pathway for substrate access from the hydrophilic exterior of MMOH in toward the active site through the α-subunit. An additional site observed for xenon binding lies at the interface of the α- and β-subunits. Once again, no rearrangement of the protein was observed upon binding at this site. The closest protein contacts are Tyr115, Thr148, and His149 from the α-subunit, and Thr53 and Val177 from the β-subunit. In the native structure, this cavity is void of any solvent.

Table 4: Xe Binding Sites in MMOH[a]

site	peak heights for Xe atoms (σ)[b]	location[c]	occupancy	B-values
1	14.9	α2, cavity 2	0.92	30.8
2	13.0	α1, cavity 2	0.91	33.7
3	6.7	α2, surface	0.30	25.7
4	6.7	α2, surface	0.20	26.4
5	6.6	α1, β1 interface	0.34	26.7
6	6.1	α2, β2 interface	0.32	26.5
7	5.5	α1, cavity 3	0.38	34.7
8	5.3	α1, cavity 2	0.28	30.5
9	5.2	α1, surface	0.26	25.5
10	n.o.[d]	α1, cavity 2	0.27	28.3
11	n.o.[d]	α1, surface	0.24	27.6

[a] Peak heights are reported only for the 2.6 Å resolution MMOH structure with Xe. [b] Peak heights are in reference to a difference map calculated with the coefficients $||F_{o,\ Xe}| - |F_{o,\ native}||$ with phases from the native structure (ref *12*). [c] α1 and α2 refer to the alpha subunit of protomers 1 and 2, respectively. [d] No significant difference electron density was initially observed for these binding sites.

Despite the observation of multiple binding sites in the α-subunit, no electron density corresponding to xenon was observed in cavity 1 at the active site. The amino acid ligands to iron adopted the orientations observed previously for oxidized MMOH and, given the limits of resolution, electron density in the cavity could only be attributed to solvent. The active site cavity has a volume of ∼185 $Å^3$, which is more than sufficient to house a xenon atom. The closest xenon atoms to the iron center, however, were those in cavity 2 and at the α/β interface located 12.7 and 11.6 Å away, respectively. The fact that xenon is not present in cavity 1 may be attributable to the absence of protein B in the crystals. This coupling protein facilitates small molecule access to the active site, although it is not yet understood how it occurs (*27*−*29*).

DISCUSSION

Cavities are present in most proteins having more than 100 amino acids, reflecting their inability to pack with 100% efficiency upon folding (*30*). Rarely does cavity volume account for more than 2.0% of overall protein volume, however, and MMOH is no exception (unpublished observations, D.A.W. and S.J.L.). The question then is, do cavities play a functional role in proteins or are they simply the consequence of imperfect folding?

Cavities have been engineered into T4 lysozyme and into synthetic four-helix bundles (*31*, *32*). The resulting structures can bind small organic molecules such as benzene or the anesthetic halothane, 2-bromo-2-chloro-1,1,1-trifluoroethane. NMR experiments using hen egg white lysozyme have detected methane and other small organic molecules in the protein interior, and these species prefer to bind hydrophobic regions (*33*). Indirect evidence exists that hydrophobic pockets in proteins are important in various metabolic reactions, since small organic molecules that bind in such

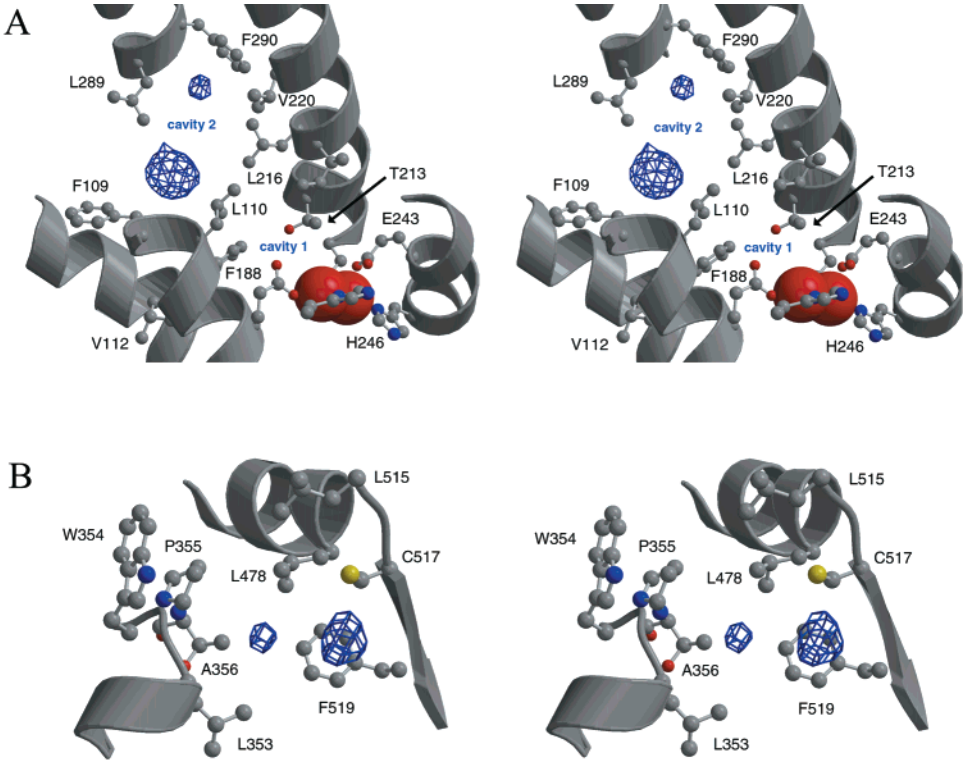

FIGURE 4: Stereoview of the xenon binding sites in (A) cavity 2 of the α-subunit, and (B) a surface pocket on the α-subunit defined by Leu405 and the residues indicated. Difference electron density peaks (blue, 7σ contour in panel A and 5σ contour in panel B) are shown for maps calculated with the Fourier coefficients $||F_o| - |F_c||$ using phases from the final model minus the xenon atoms. Iron atoms are depicted as red spheres.

cavities exert anesthetic effects on whole organisms (*34*). Indeed, many potent anesthetics are halogenated organics (*34*).

In MMOH, four independent crystal structures revealed binding of small molecules in natural hydrophobic cavities, some of which had previously been postulated to facilitate substrate access to the active site. Cavities 2 and 3 in the α-subunit, which have the greatest hydrophobic character, are the sites where these species bind most favorably. Since these cavities trace a path to the active site cavity 1, it is probable that they facilitate translocation of dioxygen, methane, and other small hydrocarbon substrates from aqueous solution to the diiron center. The low dielectric of the hydrophobic protein interior would favor such loading of these cavities.

Other proteins, including myoglobin, hemoglobin, and hydrogenase have natural cavities that may facilitate movement of nonpolar small molecules. X-ray crystal structures have revealed xenon or small organic molecule binding in myoglobin and hydrogenase (*9*, *10*, *22*), and molecular dynamics simulations with these proteins demonstrate that small molecules can move through the cavities on the picosecond time scale (*9*, *35*, *36*). The same behavior is expected for MMOH. Recent experimental evidence also links X-ray diffraction data of photodissociated CO in a mutant myoglobin to a pocket identified in previous spectroscopic and theoretical work, and argues in favor of the view that diffusion of small molecules involves the use of preexisting cavities in protein structures (*37*). Several enzymes have also been identified that facilitate substrate channeling through intramolecular tunnels (*38*). These examples provide additional evidence for how protein structures promote substrate trafficking in an efficient manner.

In contrast to myoglobin, MMOH does not have the same molecules diffusing out from the iron center that diffuse in. The products methanol and water are much more polar than either dioxygen or methane, and this difference suggests that an alternate route for product egress may exist. In support of this view, a recent structure determination of MMOH in the presence of 1 M methanol revealed no observable electron density in cavities 2 and 3 (D.A.W. and S.J.L., unpublished observations). We suggest that the flexible residues Glu243, Thr213, and Asn214 lining one side of the active site may provide a ready escape route for these polar product molecules to the protein surface. In such a scenario, the large size of MMOH provides separate regions for the efficient trafficking of substrates and products during catalysis.

In addition to its physiological substrate methane, sMMO oxidizes species as large as methyl cubane and *trans*-1-methyl-2-phenylcyclopropane (*39*, *40*). When evaluating substrate access to the active site, consideration must also be given to how such species reach the dinuclear iron center. A computational study based on the known MMOH structure indicated that substrates with volumes greater than ~71 Å^3 would not fit in the active site cavity 1 (*41*). Instead, they localized to binding sites ~14 Å from the active site, near the surface of MMOH. Protein structures are subject to conformational fluctuations that facilitate diffusion of small molecules (*42*), but it is difficult to envision large species diffusing through the cavities in the same manner as methane or dioxygen. This view is supported by the very low turnover numbers with these substrates. Consequently, a more direct

pathway from the surface of the protein, perhaps making use of the flexible amino acids cited above, may be required.

ACKNOWLEDGMENT

We thank M. Soltis and M. H. B. Stowell for valuable advice and discussion regarding xenon pressurization, A. Cohen for help at SSRL, and H. Brandstetter for aid with data collection and for useful advice and discussions. Figures 2, 3, and 4 were produced with BOBSCRIPT and RASTER3D (*43*, *44*).

REFERENCES

1. Valentine, A. M., and Lippard, S. J. (1997) *J. Chem. Soc., Dalton Trans.* 3925−3931.
2. Wallar, B. J., and Lipscomb, J. D. (1996) *Chem. Rev. 96*, 2625−2657.
3. Rosenzweig, A. C., Frederick, C. A., Lippard, S. J., and Nordlund, P. (1993) *Nature 366*, 537−543.
4. Elango, N., Radhakrishnan, R., Froland, W. A., Wallar, B. J., Earhart, C. A., Lipscomb, J. D., and Ohlendorf, D. H. (1997) *Protein Sci. 6*, 556−568.
5. Lund, J., Woodland, M. P., and Dalton, H. (1985) *Eur. J. Biochem. 147*, 297−305.
6. Green, J., and Dalton, H. (1985) *J. Biol. Chem. 260*, 15795−15801.
7. Gassner, G. T., and Lippard, S. J. (1999) *Biochemistry 38*, 12768−12785.
8. Rosenzweig, A. C., Brandstetter, H., Whittington, D. A., Nordlund, P., Lippard, S. J., and Frederick, C. A. (1997) *Proteins: Struct., Funct., Genet. 29*, 141−152.
9. Montet, Y., Amara, P., Volbeda, A., Vernede, X., Hatchikian, E. C., Field, M. J., Frey, M., and Fontecilla-Camps, J. C. (1997) *Nat. Struct. Biol. 4* 523−526.
10. Tilton, R. F., Jr., Kuntz, I. D., Jr., and Petsko, G. A. (1984) *Biochemistry 23*, 2849−2857.
11. Willems, J.-P., Valentine, A. M., Gurbiel, R., Lippard, S. J., and Hoffman, B. M. (1998) *J. Am. Chem. Soc. 120*, 9410−9416.
12. Whittington, D. A., and Lippard, S. J. (2001) *J. Am. Chem. Soc., 123*, 827−838.
13. Rosenzweig, A. C., Frederick, C. A., and Lippard, S. J. (1992) *J. Mol. Biol. 227*, 583−585.
14. Otwinowski, Z., and Minor, W. (1997) *Methods Enzymol. 276*, 307−326.
15. Brünger, A. T., Adams, P. D., Clore, G. M., DeLano, W. L., Gros, P., Grosse-Kunstleve, R. W., Jiang, J.-S., Kuszewski, J., Nilges, M., Pannu, N. S., Read, R. J., Rice, L. M., Simonson, T., and Warren, G. L. (1998) *Acta Crystallogr. D 54*, 905−921.
16. Jones, T. A., Zou, J.-Y., Cowan, S. W., and Kjeldgaard, M. (1991) *Acta Crystallogr. A 47*, 110−119.
17. Laskowski, R. A., MacArthur, M. W., Moss, D. S., and Thornton, J. M. (1993) *J. Appl. Crystallogr. 26*, 283−291.
18. Kleywegt, G. J., and Jones, T. A. (1994) *Acta Crystallogr. D 50*, 178−185.
19. Liang, J., Edelsbrunner, H., and Woodward, C. (1998) *Protein Sci. 7*, 1884−1897.
20. Soltis, S. M., Stowell, M. H. B., Wiener, M. C., Phillips Jr., G. N., and Rees, D. C. (1997) *J. Appl. Crystallogr. 30*, 190−194.
21. Verschueren, K. H. G., Seljée, F., Rozeboom, H. J., Kalk, K. H., and Dijkstra, B. W. (1993) *Nature 363*, 693−698.
22. Nunes, A. C., and Schoenborn, B. P. (1973) *Mol. Pharmacol. 9*, 835−839.
23. Schoenborn, B. P. (1976) *Proc. Natl. Acad. Sci. U.S.A. 73*, 4195−4199.
24. Gursky, O., Fontano, E., Bhyravbhatla, B., and Caspar, D. L. D. (1994) *Proc. Natl. Acad. Sci. U.S.A. 91*, 12388−12392.
25. Schiltz, M., Fourme, R., Broutin, I., and Prangé, T. (1995) *Structure 3* 309−316.
26. Prangé, T., Schiltz, M., Pernot, L., Colloc'h, N., Longhi, S., Bourguet, W., and Fourme, R. (1998) *Proteins 30*, 61−73.
27. Davydov, R., Valentine, A. M., Komar-Panicucci, S., Hoffman, B. M., and Lippard, S. J. (1999) *Biochemistry 38*, 4188−4197.
28. Liu, Y., Nesheim, J. C., Lee, S.-K., and Lipscomb, J. D. (1995) *J. Biol. Chem. 270*, 24662−24665.
29. Pulver, S. C., Froland, W. A., Lipscomb, J. D., and Solomon, E. I. (1997) *J. Am. Chem. Soc. 119*, 387−395.
30. Hubbard, S. J., Gross, K.-H., and Argos, P. (1994) *Protein Eng. 7* 613−626.
31. Baldwin, E., Baase, W. A., Zhang, X. J., Feher, V., and Matthews, B. W. (1998) *J. Mol. Biol. 277*, 467−485.
32. Johansson, J. S., Gibney, B. R., Rabanal, F., Reddy, K. S., and Dutton, P. L. (1998) *Biochemistry 37*, 1421−1429.
33. Otting, G., Liepinsh, E., Halle, B., and Frey, U. (1997) *Nat. Struct. Biol. 4*, 396−404.
34. Eckenhoff, R. G., and Johansson, J. S. (1997) *Pharmacol. Rev. 49*, 343−367.
35. Elber, R., and Karplus, M. (1990) *J. Am. Chem. Soc. 112*, 9161−9175.
36. Carlson, M. L., Regan, R. M., and Gibson, Q. H. (1996) *Biochemistry 35*, 1125−1136.
37. Brunori, M., Vallone, B., Cutruzzola, F., Travaglini-Allocatelli, C., Berendzen, J., Chu, K., Sweet, R. M., and Schlichting, I. (2000) *Proc. Natl. Acad. Sci. U.S.A. 97*, 2058−2063.
38. Miles, E. W., Rhee, S., and Davies, D. R. (1999) *J. Biol. Chem. 274*, 12193−12196.
39. Choi, S.-Y., Eaton, P. E., Kopp, D. A., Lippard, S. J., Newcomb, M., and Shen, R. (1999) *J. Am. Chem. Soc. 121*, 12198−12199.
40. Valentine, A. M., LeTadic-Biadatti, M.-H., Toy, P. H., Newcomb, M., and Lippard, S. J. (1999) *J. Biol. Chem. 274*, 10771−10776.
41. George, A. R., Wilkins, P. C., and Dalton, H. (1996) *J. Mol. Catal. B: Enzym. 2*, 103−113.
42. Lakowicz, J. R., and Weber, G. (1973) *Biochemistry 12*, 4171−4179.
43. Esnouf, R. M. (1997) *J. Mol. Graph. & Modell. 15*, 132−134.
44. Merritt, E. A., and Murphy, M. E. P. (1994) *Acta Crystallogr. D 50*, 869−873.

BI0022487